

Effect of Faraday Rotation on L-band Interferometric and Polarimetric Synthetic-Aperture Radar Data

Eric Rignot

Jet Propulsion Laboratory, California Institute of Technology, 4800 Oak Grove Drive,
Pasadena CA 91109-8099.

Abstract. Electromagnetic waves travelling through the ionosphere undergo Faraday rotation of the polarization vector which modifies the polarization and phase characteristics of the electromagnetic signal. Using L-band ($\lambda = 24$ cm), polarimetric, Synthetic-Aperture Radar (SAR) data from the Shuttle Imaging Radar C- (SIR-C) mission of 1994, we synthesize the effect of Faraday rotation on actual interferometric and polarimetric data. We find that the temporal coherence of the interferometric phase is reduced by 20 percent when Faraday rotation changes by 40° between successive passes of the radar system. In addition, when Faraday rotation changes by more than 60° , a differential phase signal exhibiting homogeneous spatial variations appears in the interferogram which impairs the mapping of surface topography or the detection of ground motion. This differential phase signal is attributed to wavelength-sized differences in penetration depth of horizontal- and vertical-polarized radar signals through intermediate levels of vegetation canopy. In another experiment, we compare SAR data from the Japanese JERS-1 L-band instrument acquired over area of active deforestation in Rondonia, Brazil with SIR-C L-band SAR data acquired at the same incidence, only a few weeks apart, but from a lower orbit around the Earth. Significant differences in scattering behavior are recorded between the two datasets in areas of slash and burn forest, which cannot be attributed to surface change. The difference in radar backscatter is however consistent with a Faraday rotation of 30 - 45° in the JERS data and no Faraday rotation in the SIR-C data, as expected from standard ionosphere models. During ionospheric storms, or in between solar maxima, ionospheric perturbations could be more severe. In the case of single channel data collected by JERS-1, no data correction is possible. Data correction requires the full polarimetric information.

Submitted to IEE Trans. Geosc. Rem. Sens., Jan. 30, 1998.

Introduction

Electromagnetic waves travelling through the ionosphere interact with the electrons and the magnetic field with the result that the polarization vector of the electric field is rotated by an angle, ψ , called the Faraday rotation (Davies, 1965). Other effects of the ionosphere include propagation delays of the radar echoes, ray bending, and phase changes (Thompson et al., 1986). These effects are of importance for the processing of multi-channel and interferometric Synthetic-Aperture Radar (SAR) data, but here we will only discuss the effect of Faraday rotation on polarimetric and interferometric data.

Faraday rotation is proportional to the square of the radar wavelength, λ^2 , to the Total Electron Content of the ionosphere, TEC, and to the Earth's magnetic field, B_o (Davies, 1965). Hence, the effect is more effective at the long radar wavelengths (a few tens of centimeters) than at the shorter wavelengths (a few centimeters). It is 16 times larger at L-band (24-cm wavelength) compared to C-band (5.6-cm wavelength). Faraday rotation also varies by one order of magnitude between day and night as solar illumination exerts a major control on the level of ionospheric activity. Finally, Faraday rotation varies with latitude and is larger at the tropics than at the poles.

The peak ionospheric activity occurs at about 400 km altitude (Fig.1). Low-orbiting (200-km altitude) radar systems of the class of the Shuttle Imaging Radar C- (SIR-C) are not expected to be effected by the ionosphere. SARs of the class of the Japanese Earth Resource Satellite (JERS), an L-band SAR orbiting at 800 km altitude, however, send and receive radar signals through most of the ionosphere. The effect should be negligible at C-band frequency (at this frequency, a typical value of the Faraday rotation is just a few degrees during the day, which is about the noise level of the phase measurements); but not at L-band or lower frequencies.

Radar astronomers solved the problem long ago by operating ground-based radars at circular polarization to probe planetary objects (Evans, 1960). Faraday rotation is not a factor at circular polarization. For monitoring of the Earth's surface, however, operating a radar at circular polarization may or may not be optimal for the retrieval of geophysical parameters such as vegetation growth or soil moisture because these techniques tend to require the full Stokes matrix for each resolution element. In addition, these techniques are being developed using spaceborne/airborne SARs operating at linear polarization.

In the case of a linear-polarized radar system, e.g. JERS-1's L-band HH-polarized (horizontal transmit and receive) system, the effect of Faraday rotation will be to rotate the polarization vector of the electric field by an angle ψ one way during transmission of the signal through the ionosphere and by an angle $-\psi$ the other way during reception of the signals scattered from below the ionosphere. In effect, the radar system will act as a linear-polarized system operating at XX-polarization, where X is a vector at an angle ψ above the horizontal polarization axis (Fig.2). At that polarization, the scattering properties of the surface will be different, so the scientific interpretation and utilization of the radar backscatter data will be effected. Similarly, if the amount of Faraday rotation varies from one passage of the satellite to the next, it will effect the quality of repeat-pass SAR interferograms or the interpretability of recorded temporal changes in radar backscatter in terms of surface changes.

In this study, we use data from low and high-orbiting satellites to try to determine the impact of Faraday rotation on practical applications of radar interferometry and polarimetry at the L-band frequency. We determine the influence of changes in ionospheric activity on the temporal coherence of the phase signal and on the inference of geophysical quantities from the radar backscatter values and the phase signal. We also compare radar data acquired by SIR-C and JERS at the same site, same time of year, and same incidence but from different

orbiting altitudes. Based on the results, we provide some conclusions on the expected effect of the ionosphere on current or future high-orbiting spaceborne L-band SAR data.

Methods

Faraday rotation may vary both temporally and spatially. Here we will ignore possible spatial variations in ionospheric activity across a SAR scene and will only consider the effect of changes in the amount of Faraday rotation uniformly across a whole scene. To synthesize full scattering matrices recorded by an imaging polarimeter, here SIR-C, and synthesize the response of the surface at XX-polarization to mimic the data which would be recorded by a spaceborne L-band SAR operating at HH-polarization above a spatially uniform ionosphere with Faraday rotation characteristics as shown in Fig.2.

From this synthesis, we study two aspects of Faraday rotation. One aspect is how the phase rotation reduces the temporal coherence and physical nature of the interferometric phase measured from data acquired at different epochs. A second aspect is to determine how a changing ionosphere will affect the interpretability of the data in terms of surface processes. For the first aspect, we use SIR-C data acquired in the Mahantango Creek Watershed in the U.S. for which polarimetric and interferometric L-band data were available. For the second one, we compare SIR-C polarimetric L-band data from a test site in Rondonia, Brazil with SAR data acquired a few weeks earlier and one year later by the JERS-1 SAR instrument.

Study Sites

The Mahantango Creek Watershed SIR-C hydrology test site is located at 76.6° west, 40.7° north, in the state of Pennsylvania, U.S.. The site is in the Valley and Ridge province of eastern Pennsylvania, near the city of Sunbury, PA. It is an area of adjacent valleys and ridges resulting from the formation of the Appalachian mountain several hundred million

years ago. Ridge tops are forest-covered. Valleys comprise cleared land and farm fields. The 11 km x 50 km scene shown in Fig. 3a was acquired at 46° incidence angle, during orbit 150 of SIR-C, on Oct. 9, 1994, at 10:08 am local time, at both L- and C-band fully polarimetric (only the L-band HH data are shown in Fig. 3a).

The second site is located 50 km south-east of the city of Porto Velho, in the state of Rondonia Brazil, in an area of active deforestation which we studied previously using SIR-C, JERS, Landsat and SPOT data (Rignot and others, 1997). The region is traversed by highway BR-364, which opened in 1984, and started most of the deforestation activities. Much of the land is now in pasture of various quality for cattle, and secondary growth of various ages. SIR-C data were collected over that site at 02:18 am local time, during orbit 94 of SIR-C, at a center location of 8 deg 58' south, 63 deg 17' west on Oct. 6, 1994, at an incidence angle of 37° at the image center, with C- and L-band fully polarimetric. The same area was imaged on Oct. 5, 1993, Sept. 22, 1994 and Oct. 23, 1995 by the JERS SAR which operates at 35° incidence, L-band HH-polarization. Sept.-Oct. corresponds to the peak of the dry season in Rondonia, which is the time of year when most land clearance occurs. JERS and SIR-C data were acquired at the same frequency, same incidence, but different orbiting altitudes (Fig. 1).

Interferometric Results

A radar interferogram of the Mahantango Creek Watershed generated at L-band HH-polarization is shown in Fig. 3b using data collected one day apart. The component of the interferometric baseline perpendicular to the line of sight of the radar, B_\perp , is 60 m. The altitude of ambiguity of the phase data is 450 m, meaning that each interferometric fringe in the interferogram represents a 450-m changes in surface elevation. Comparing this interferometric map with a topographic map of the area produced by the U.S.G.S. yields a

r.m.s. error in surface elevation of 10-20 m. The interferometric map obtained at C-band - not shown here - yielded a phase coherence level which was too low to convert the data into a height map.

Fig. 3d-f show how the interferometric fringes evolve as the amount of Faraday rotation changes by $\Delta\psi = 30, 45, 60$ and 90 degrees from one day to the next (the first day is assumed to be HH-polarized, the second day is assumed to be XX-polarized). When $\Delta\psi > 30^\circ$, the phase noise increases over most of the scene. The reduction in fringe visibility is more apparent in Fig. 4c-e as $\Delta\psi$ increases. The reduction is largest for $\Delta\psi = 90^\circ$. Perhaps more important, the fringe pattern changes as $\Delta\psi$ increases. The effect is most noticeable for $\Delta\psi > 60^\circ$ (look for instance in the ovale-shaped valley area in the center of the scene).

To illustrate the change in phase signal quoted above, we removed the topographic map obtained from the L-band HH-polarization data collected on both days from the interferogram shown in Fig. 3f, which was obtained combining the L-band HH-polarized data on the first day and the L-band XX-polarized data on the second day with $\Delta\psi = 90^\circ$ (meaning L-band VV-polarized data on the second day). The result is a differential phase signal, about $1/3$ of a cycle in magnitude, which homogeneously varies from field to field (Fig. 3g). Fields exhibiting little or no differential phase signal tend to correspond to bare surfaces, whereas fields exhibiting large phase differences correspond to crops. Exceptions to this rule may exist as we were not able to verify the land cover of each individual field. Forested areas developing on the valley ridges have a different behavior depending on whether the terrain slope is facing the radar illumination or facing away from the radar illumination.

The decrease in phase coherence associated with the change in Faraday rotation is plotted in Fig. 4. Phase coherence is reduced by 20 percent when $\Delta\psi = 40^\circ$. Note that phase coherence is not destroyed for $\Delta\psi = 90^\circ$, which means that the scattering centers are not

fundamentally different at both polarizations. There is however a difference in scattering pathlength between H- and V-polarized signals since we detected a non-zero differential phase between the two. Also, it is important to note that phase coherence is more dramatically reduced over forested areas (ridges and portions of the valley) than on crops (valleys).

These results suggest that a major change in Faraday rotation will not necessarily destroy phase coherence at L-band based on Faraday rotation alone, but it will certainly reduce it. More important, it will change the nature of the phase signal. If the interferogram shown in Fig. 3f were to be used to generate a topographic map, the height error would increase by several hundred meters from field to field due to the phase differential between H- and V-polarized signals. Similarly, if the interferogram in Fig. 3f were to be used to detect ground motion, it would detect a signal of about $1/3$ of a cycle which does not correspond to an actual motion of the ground but to a difference in electric pathlength between H- and V-polarized signals.

Our interpretation of the L-band results is that radar scattering at that frequency is dominated by the ground layers for bare fields and crops; and by the ground, the branches and the tree-trunks for forests at both H- and V-polarizations. The difference in scattering pathlength may result from the fact that H-polarized signals penetrate the vegetation canopy (essentially deeper) with less attenuation than V-polarized signals. If this interpretation is correct, the scattering centers at V-polarization should always be above those at H-polarization, meaning that the phase differential between day 2 and day 1 should be positive. This is indeed what we observe (the phase in Fig. 3 increases from blue to red, yellow and blue again when the radar distance to the radar decreases, meaning the scatterers centers get closer to the radar in the slave image (XX-polarization) than in the reference image (HH-polarization)).

Over forested terrain, the difference in scattering pathlength is probably related to the influence of terrain slope on the scattering term corresponding to ground-trunk double bouncing. As discussed by van Zyl (1993), H-polarization is more sensitive to changes in ground slope than V-polarization in ground-trunk scattering interactions, and a positive tilt of the surface toward the radar illumination has the same effect than a negative tilt. In the SIR-C image, there is indeed no difference in differential phase between hills facing the radar and those away from the radar. The ridge tops, where the surface tilt is presumably very small, show a higher degree of phase coherence than the sides of the ridges.

SIR-C, JERS Comparison

Figure 5 shows a comparison between a SIR-C image acquired at L-band HH-polarization, a JERS image acquired a couple of weeks earlier at the same frequency and polarization, and a JERS image acquired one year later.

The two instruments operate nearly at the same incidence angle, same radar frequency and polarization. The bright patches of cleared forests appearing in the SIR-C images were identified in the field as associated with slash and burn areas, meaning areas where the forest had been cut and burned for the first time, leaving a complex chaos of burned and semi-burned trees, most of them laying flat on the ground, with only a few remaining standing trees (Rignot and others, 1997). These cleared areas are typically abandoned for a year until they are burned again. The process is repeated several times before the land is transformed into pasture.

In the SIR-C data, the radar backscatter from slash and burn areas is brighter than the forest at HH-polarization because of the preferred horizontal polarization of the scatterers (downed tree-trunks), an effect which is consistent with model simulations of the scattered

field from an ensemble of discrete, dielectric, cylinders (Bohren and Huffman, 1983). This phenomena was first observed in SIR-B data of the Amazon (Stone and Woodwell, 1988). In contrast, the same areas are for the most part darker in radar backscatter than the surrounding forest in the 1994 and 1995 JERS images. We verified in the field in Oct. 1995 that most slash and burn areas were still in some stage of clearing/re-burning, with a large number of dead trunks covering the ground, a year after the SIR-C overflight. Hence the difference in scattering behavior between SIR-C and JERS cannot be attributed to the removal of tree trunks.

Figure 6 shows a simulation of what an L-band HH image would look like for various degrees of Faraday rotation if SIR-C were flying at 800-km altitude. Note how the bright radar signature of slash and burn areas progressively disappears to be replaced by a dark radar signature at VV-polarization. Similarly, flooded areas marked in Fig. 6a in the top left portion of the scene change dramatically in radar backscatter. The dark radar signature at VV-polarization is consistent with the fact that most tree trunks laying on the ground acts as discrete horizontal dielectric cylinders with strong scattering at H-polarization and weak scattering at V-polarization (van Zyl, 1993).

Hence, the simulation suggests that JERS-1 data acquired a few weeks prior to the SIR-C flight resemble the SIR-C data with a Faraday rotation of 30-45°. For instance the area of slash and burn marked at the bottom of Fig.6a appear darker than Fig. 6a in Fig.5b, but yet not as dark as in Fig.6e-f. The 1995 data show even less contrast between slash and burn areas and the surrounding forest, which would suggest a Faraday rotation closer to 45° than 30°. In that case however, the change could also be due to surface changes, for instance vegetation regrowth after one year may attenuate radar scattering from the horizontal dead trunks.

It was expected that SIR-C data would not be sensitive to Faraday rotation because SIR-C orbited below most of the ionosphere. Indeed, a low level of cross-talk between H- and V-channels (-33dB) was consistently measured during both SIR-C experiments, day and night (Freeman and others, 1995), which would not have been the case in the presence of Faraday rotation. In contrast, data acquired at 800-km altitude at L-band frequency by JERS-1 are expected to be effected by Faraday rotation according to both standard ionosphere models as well as long time experience with Global Positioning System (GPS) data (which uses a dual-frequency system to get rid of ionospheric effects).

If these conclusions are correct, they explain why the range in radar backscatter recorded by JERS-1 SAR over tree stands of various biomass is only of 2-3 dBs (MITI, 1995), whereas airborne experiments suggested a range of variation in radar backscatter of about 6 dB (Dobson and others, 1992). Similarly, the increase in radar backscatter of forest regrowth in the Amazon is less than that expected from airborne experiments (Luckman and others, 1997) and most JERS data do not exhibit the bright radar signature of recent slash and burn areas observed with both SIR-B and SIR-C over large areas. The JERS-1 results are more consistent with the AIRSAR L-band VV-polarization results (Dobson and others, 1992), which is less sensitive to woody biomass.

On the relevance of the simulations

Figure 7 shows how the level of ionospheric activity, measured by the TEC from GPS data, varies from year to year and increases with the level of solar activity (Klobuchar and Doherty, 1997). The TEC varies from month to month, and even from day to day within the same month. Faraday rotation is directly proportional to the TEC (Davies, 1965). Most satellite SARs operate in a sun-synchronous mode and obtain repeat-pass acquisitions of the same site at about noon local time during descending passes, which is the peak ionospheric

activity; or around midnight local time for the ascending passes, which is the minimum ionospheric activity. Variations in ionospheric activity from day to day or month to month can be large as shown in Fig. 7, especially near solar maximum (1990 was the last solar maximum).

Assuming a maximum Faraday rotation of 37° at L-band from the standard ionosphere model of Evans and Hagfors (1968) with a TEC of $5 \cdot 10^{17}$ elec/m² during the day, the results in Fig. 7 suggests that Faraday rotation could double during solar maximum and reach 74° , which would then create serious problems in the interpretation of the data according to our SIR-C results. Outside of the period of solar maximum, the TEC may vary anywhere between 10^{17} elec/m² and $5 \cdot 10^{17}$ elec/m² at noon, which translates into relative variations in Faraday rotation of about 30° . This is at the limit of causing significant disturbances in the amplitude and phase signal according to our study, so these fluctuations should not create major interpretation problems with the data. Yet, Fig. 7 also shows episodic events, or ionospheric storms, for which the TEC increases even more over a short period (check for instance the plot for January 1988), in which case we do expect problems interpreting the data.

Based on our assumption of a "standard" Faraday rotation of $30\text{-}40^\circ$, we conclude that Faraday rotation will be a problem for monitoring surface changes at L-band when data are acquired near the solar maximum, or during episodic ionospheric storm events.

Conclusions

Using real SAR data from the SIR-C and JERS-1 mission, we quantified the influence of changes in ionospheric activity on polarimetric and interferometric SAR at the L-band frequency. We find that Faraday rotation of several tens of degrees significantly changes the

radar amplitude and phase characteristics of remotely sensed surfaces, and that the time variability of the phenomena may be a limiting factor for change detection and interferometry applications. Existing records of ionospheric activity suggest that large variations in ionospheric activity exist on a daily to a yearly time scale. Near the solar maximum or during ionospheric storms, high-orbiting spaceborne radar systems operating at L-band will be effected by Faraday rotation of several tens of degrees larger than usual. Anyone using uncorrected data should therefore be concerned about this effect.

To circumvent this limitation, one possibility is to design and operate the radar at circular polarization, as commonly done in radar astronomy. Most research work conducted using earth-borne SARs however is based on using linear polarization data. A second solution is to operate the radar at a higher radar frequency, for instance S-band (10-cm wavelength) instead of L-band (24-cm wavelength) and thereby reduce the magnitude of the disturbance by a factor 5.8. Our experience with S-band data is however limited, except for data acquired by the Almaz SAR system on Earth and the Magellan Radar System on Venus. A third possibility is to estimate the amount of ionospheric activity, for instance using ground stations or GPS data or SAR data (processed at slightly offset frequencies), and use those estimate to throw out bad data with unusual high levels of ionospheric activity. Whatever the estimation technique, however, the "true" polarization of the data cannot be restituted because that operation requires the full scattering matrix (Davies, 1965; Gail, 1995); and researchers interested in differential interferometry applications will detect phase changes which have nothing to do with surface changes. A fourth and probably best solution is to operate the radar in full polarimetric mode. In that case, Faraday rotation - as well as other effects of the ionosphere - may be estimated completely from the data, the true polarization signature of the surface may be restituted, and the true interferometric signal may be reconstructed.

Acknowledgements

This work was performed at the Jet Propulsion Laboratory under a contract with the National Aeronautics and Space Administration. I would like to thank my JPL colleagues Jakob van Zyl, Gilles Peltzer and Paul Rosen for stimulating discussions about this topic, Tony Mannucci at JPL for mentioning the recent work of Pat Doherty at the Institute for Scientific Research, Boston College and Jack Klobuchar, at Total Electronic Concepts, Lincoln, MA, and Pat Doherty for generously providing the plot in Figure 7 in advance of publication.

References

- Bohren, C. F., and D. R. Huffman. 1983. *Absorption and Scattering of Light by Small Particles*, John Wiley, New York.
- Davies, K. 1965. *Ionospheric radio propagation*, United States Department of Commerce, 210-2145.
- Dobson, M.C., Ulaby, F.T., LeToan, T., Beaudoin, A., Kasischke, E.S., and Christensen, N. 1992. Dependence of radar backscatter on conifer forest biomass, *IEEE Trans. Geosc. Rem. Sensing* **30**, 412-415.
- Dubois, P., J. van Zyl, and T. Engman. 1995. Measuring soil moisture with imaging radars, *IEEE Trans. Geosc. Rem. Sens.* **33**(4), 915-926.
- Evans, J.V. 1960. Radar Astronomy, *Comtemp. Phys.* **2**, 116.
- Freeman, A. and 8 others. 1995. SIR-C data quality and calibration results, *IEEE Trans. Geosc. Rem. Sens.*, **33**(4), 848-857.
- Gail, W.B. 1997. Effect of Faraday rotation on polarimetric SAR, *IEEE Trans. Aerosp. Electron. Sys.*, in press.
- Klobuchar, J. A., and P. H. Doherty. 1997. Expected Ionospheric Effects on GPS Signals in the Year 2000, *GPS Solutions*, in press.
- Luckman, A., Baker, J., Kuplich, T.M., Yanasse, C.D.F. and Frery, A.C. 1997. A study of the relationship between radar backscatter and regenerating tropical forest biomass for spaceborne SAR instruments, *Rem. Sens. Environ.*, **60**(1), 1-13.
- Ministry of International Trade and Industry, NASDA, 1995. Final report of JERS-1/ERS-1 system verification program, Volume II, March 1995.
- Rignot, E., R. Zimmerman, J. van Zyl and R. Oren. 1995. Spaceborne applications of a P-band imaging radar for mapping of forest biomass, *IEEE Trans. Geosc. Rem. Sens.*, **33**(5), 1162-1169.
- Rignot, E., W. Salas, and D. Skole. 1997. Mapping deforestation and secondary growth in Rondonia, Brazil using imaging radar and thematic mapper data, *Rem. Sens. Environ.*, **59**, 167-179.
- Stone, T.A. and Woodwell, G.M. 1988. Shuttle imaging radar A analysis of land use in Amazonia, *Int. J. Rem. Sens.* **9**, 95-105.
- Thompson, A.R., J.M. Moran, and G.W. Swenson. 1986. *Interferometry and synthesis in*

radio astronomy, Wiley Interscience, New York.

van Zyl, J.J. 1993. The effect of topography on radar scattering from vegetated areas, *IEEE Trans. Geosc. Rem. Sens.* **31**(1), 153-160.

Figures

Figure 1. International Reference Ionosphere (1985) calculation of the electron density height profile for a variety of latitudes and at midnight and noon. Longitude is 293° east; latitudes are 20° (solid line), 40° (dotted), 60° (dashed) and 80° (long dashed) north (Adapted from Evans and Hagfors, 1968). Arrows denote the orbiting altitude of SIR-C and JERS-1.

Figure 2. Rotation of the polarization vector, \mathbf{E} , due to a Faraday rotation of ψ . The result of transmitting and receiving through the ionosphere is to transform an HH-polarization system (H means horizontal) into an XX-polarization system, with the polarization vector \mathbf{X} being oriented ψ from the horizontal.

Figure 3. SIR-C image data of the Mahantango Creek Watershed, Pennsylvania located at 76.6° west, 40.7° north. The scene is 11 km x 50 km in size, acquired at 46° incidence angle, during orbit 150 of SIR-C, on Oct. 9, 1994, at 10:08 am local time. (a) Amplitude image at L-band HH-polarization; (b) Radar interferogram generating combining L-band HH-polarized data acquired on Oct. 9 and 10. Each fringe or full color cycle represents a 360° variation in phase, here equivalent to a 450-m change in surface elevation. Interferograms combining L-band HH on Oct. 9 and L-band XX on Oct. 10 with ψ equal to (c) 30° , (d) 45° , (e) 60° , and (f) 90° (equiv. to L-band VV-polarization). The color intensity of each one of these interferograms is modulated by the coherence of the phase signal. Areas of low coherence have a darkened tone. Phase coherence is decreasing from (b) to (f). (g) Interferogram showing the differential phase signal between L-band HH on Oct. 9 and L-band VV on Oct. 10 after removal of the topographic map obtained combining L-band HH on Oct. 9 and L-band HH on Oct. 10. Note the correlation between the patches of homogeneous variation in phase and the field delineated in the radar amplitude image (a).

Figure 4. Decrease in phase coherence of the radar interferogram shown in Fig. 3 when the angle of the Faraday rotation increases from 0 (Fig.3b) to 90° (Fig.3f).

Figure 5. Radar amplitude image of a deforestation test site in the state of Rondonia, Brazil, located 50 km south-east of the city of Porto Velho, at 8 deg 58' south, and 63 deg 17' west. (a) L-band HH SIR-C image acquired on Oct. 7, 1994. Image size is 20.7 km by 25 km. (b) L-band HH JERS image acquired on Sept. 22, 1994; and (c) L-band HH JERS image acquired on Oct.23, 1995.

Figure 6. Simulation of the effect of Faraday rotation on SIR-C data of the deforestation test site in Rondonia, Brazil. Fig.5a shows the radar amplitude image at L-band HH-polarization, meaning no Faraday rotation. Radar amplitude image for a Faraday rotation of $\psi =$ (a) 0° , (b) 30° , (c) 45° , (d) 60° , (e) 75° and (f) 90° (equiv. to L-band VV-

polarization). Areas of slash and burn (radar bright in (a)) progressively become darker than the surrounding forest when the polarization vector is rotated.

Figure 7. Long-term plot of Total Electron Content (TEC) from Hamilton, MA (38.7 N, 70.7 W) near vertical incidence. Each chart is a plot of diurnal TEC behavior for each day in the month indicated. Dependence on solar cycle is displayed from left to right (solar minimum in 1986 to maximum in 1990). Seasonal dependence for a given year is displayed from top to bottom. This plot was obtained courtesy of Pat Doherty and Jack Klobuchar.

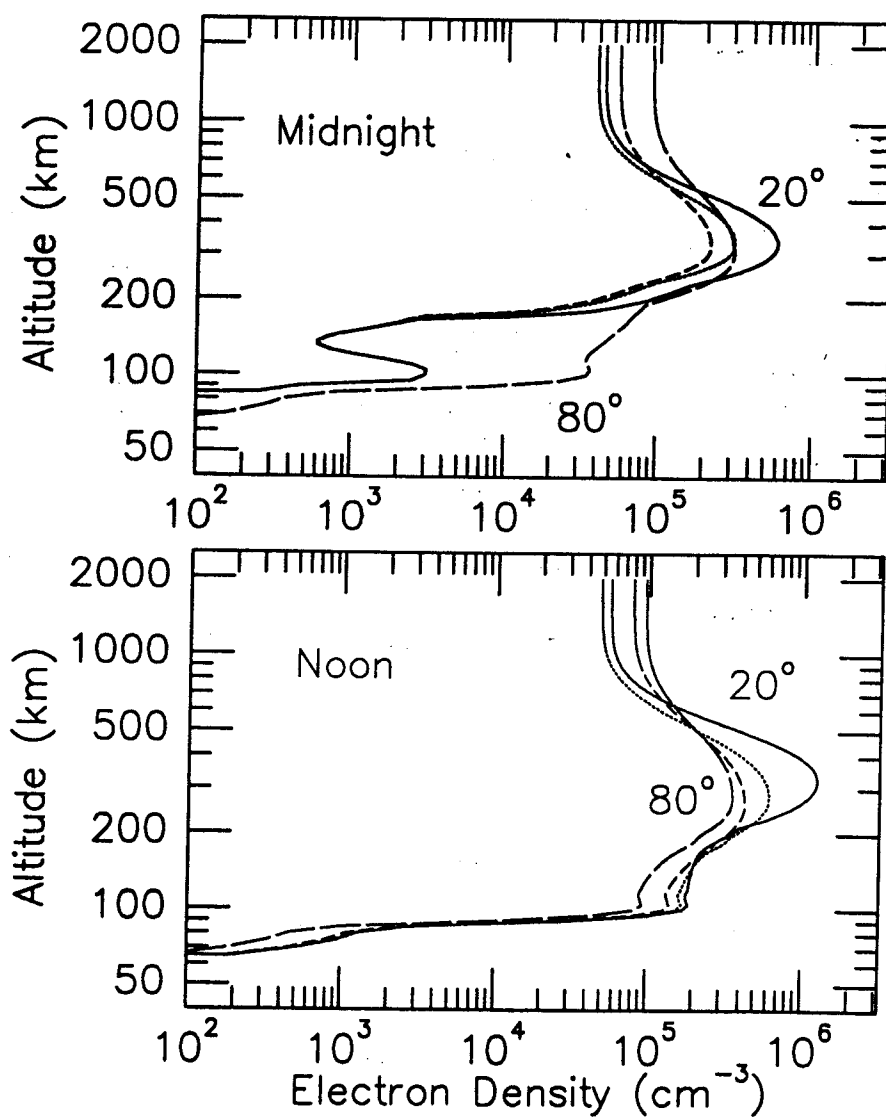


Figure 2

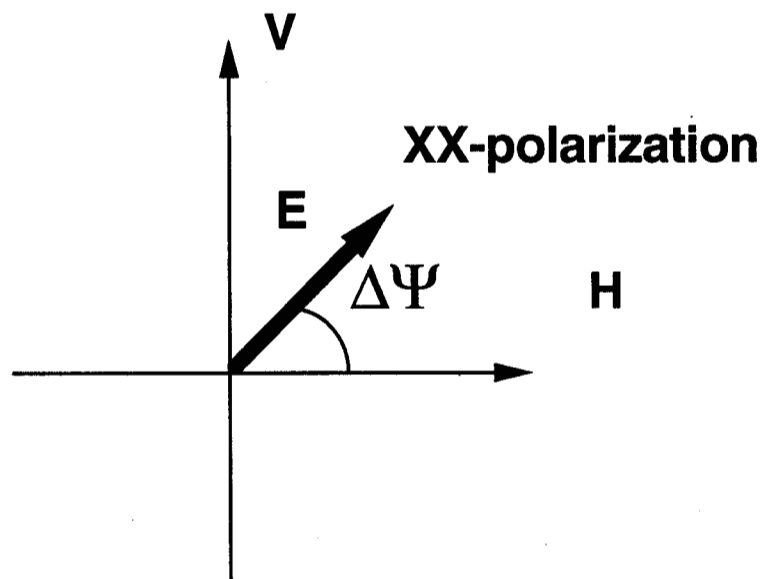
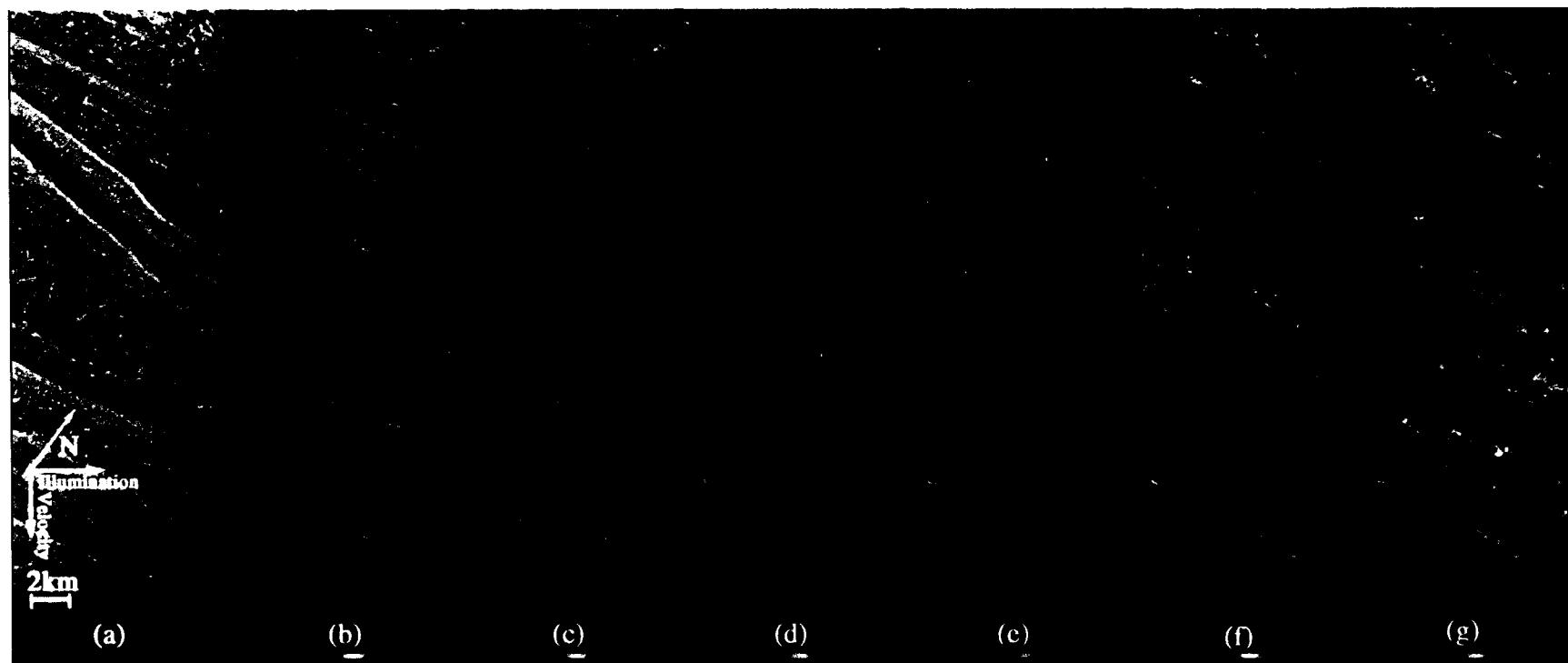


Figure 2

FIGURE 3



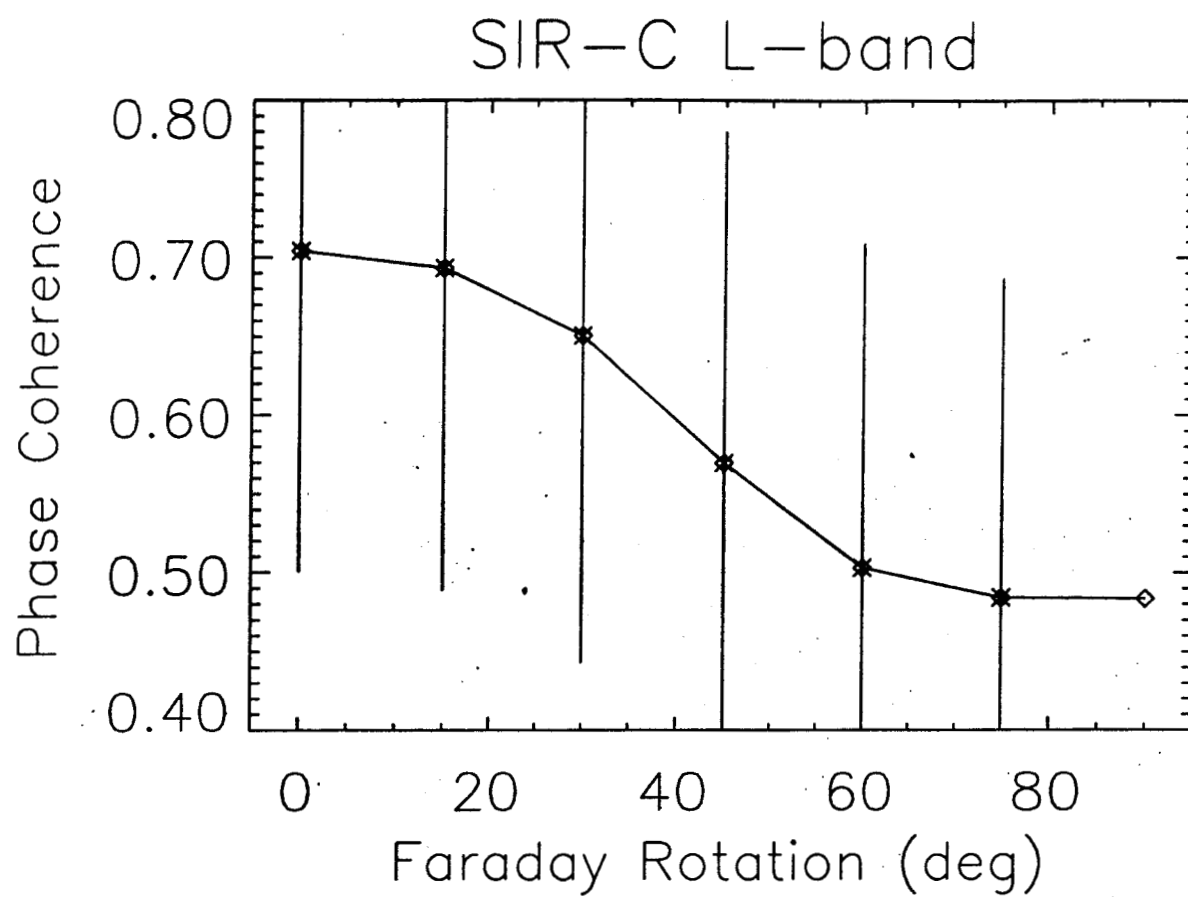


Figure 4.

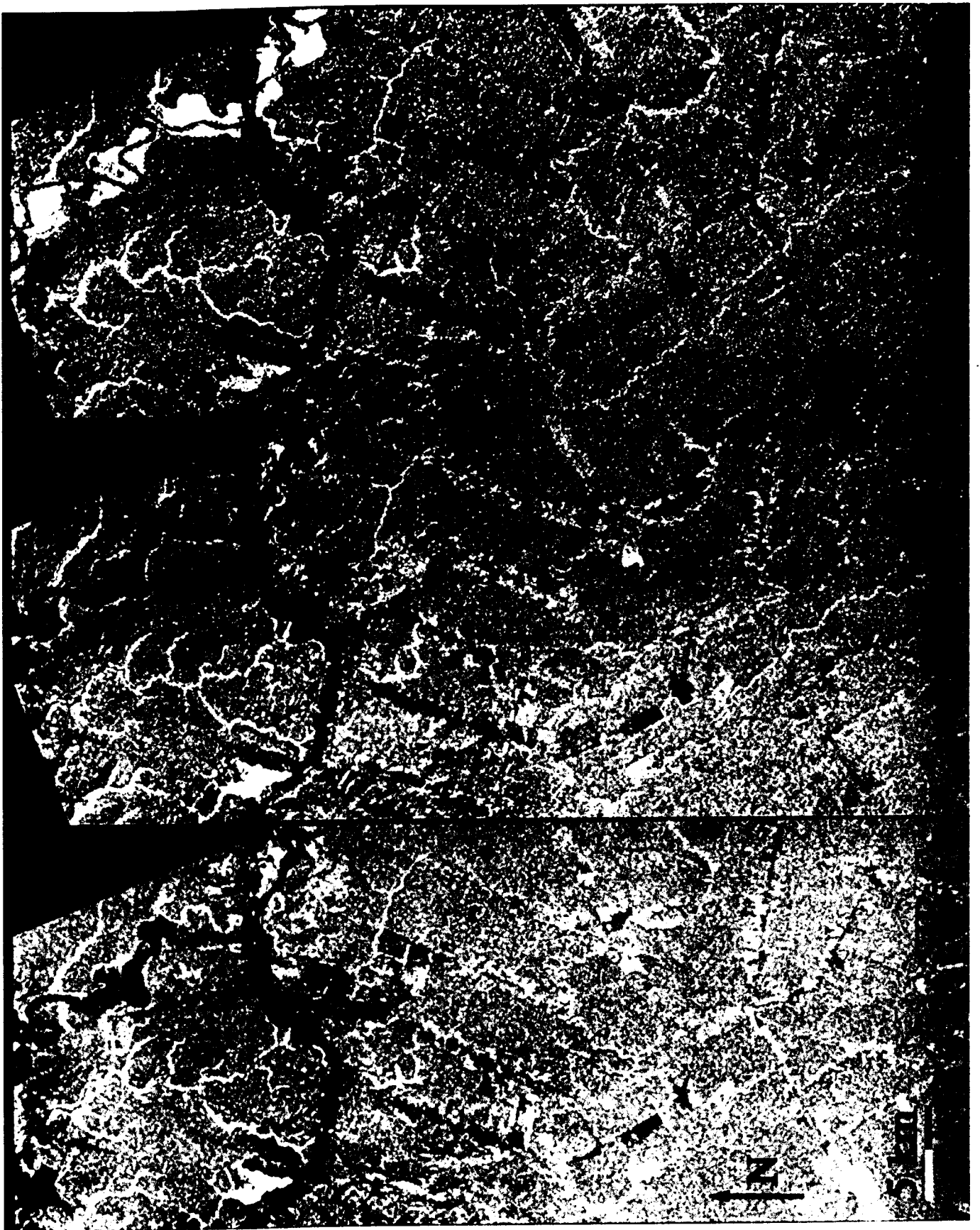


Figure 5.

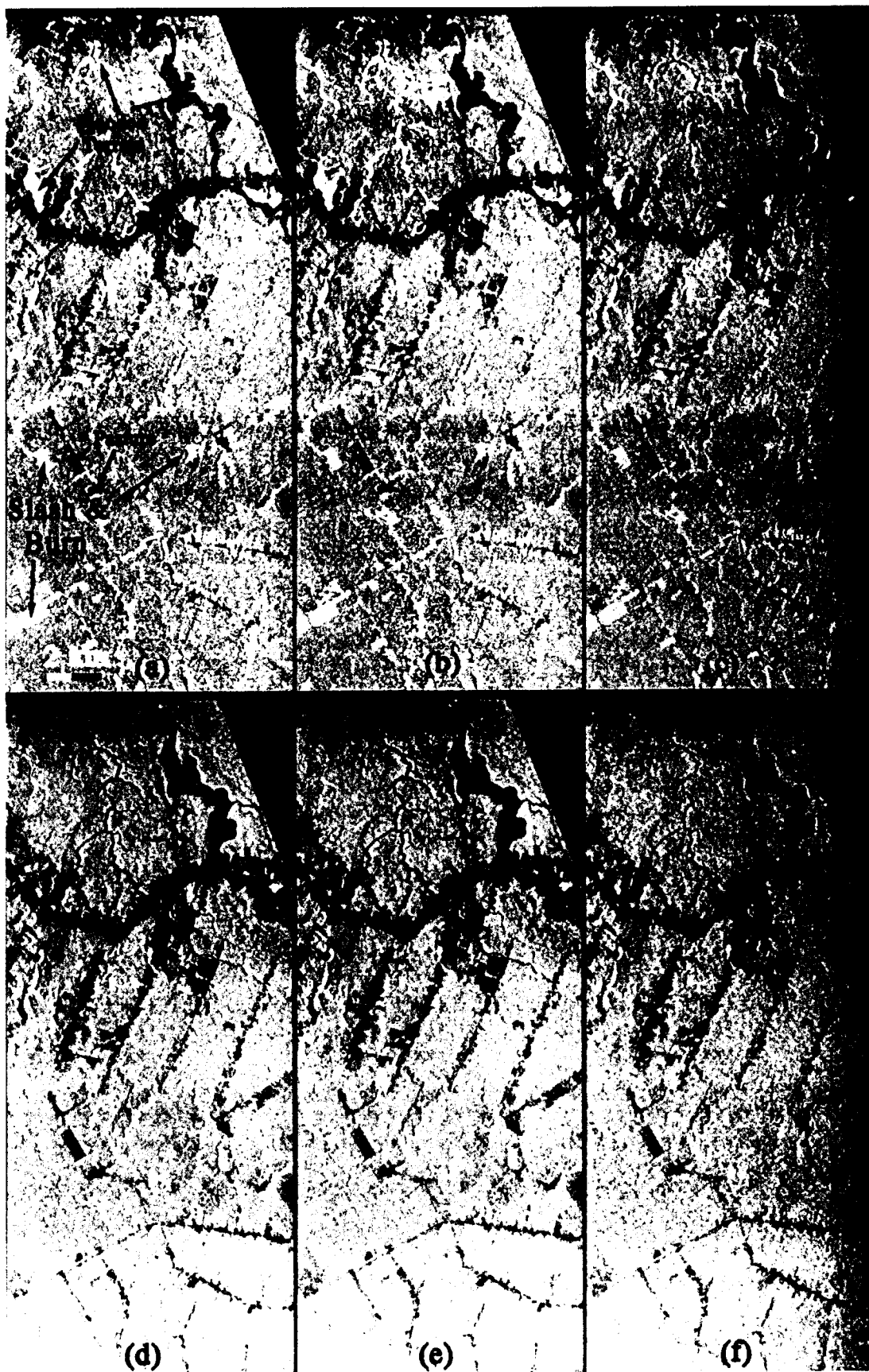


Figure 6

HAMILTON, MA TEC vs MONTHLY MEAN SOLAR FLUX

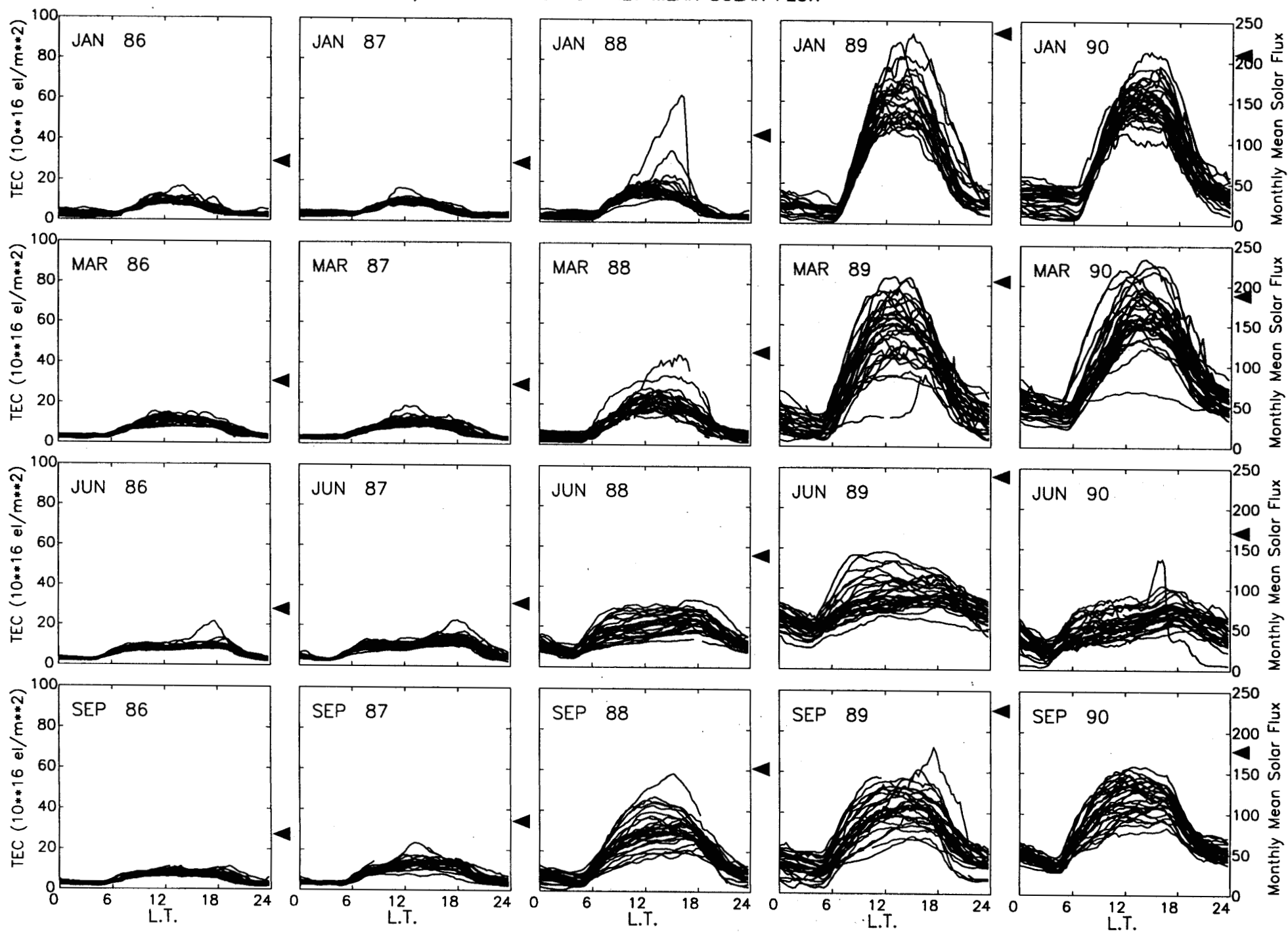


Figure 7.